Electronic Supplementary Information

Photostable wide-bandgap perovskites with enhanced interface coupling for all-perovskite tandems

Chunyan Li[†ab], Yao Zhang[†*ab], Haiyan Zhao[ab], Jixiang Zhang[abc], Zhongxun Yu[abc], Xiaoan Tang[ab], Yudong Wang[ab], Han Chen*[abd]

Affiliations

[a] State Key Laboratory of Metal Matrix Composites, Shanghai Jiao Tong University, Shanghai, China.

[b] Innovation Center for Future Materials, Zhangjiang Institute for Advanced Study, Shanghai Jiao Tong University, Shanghai, China.

[c] Shanghai Jiao Tong University JA Technology New Energy Materials Joint Research Center, Shanghai, China.

[d] Joint Research Center for Clean Energy Materials, Shanghai Jiao Tong University, Shanghai, China.

[†]These authors contributed equally.

*Correspondence: blinkdagger@sjtu.edu.cn; chen.han@sjtu.edu.cn

Experimental Section

Computational method

DFT simulations of the molecules were conducted using the ORCA 5.0.3 package[1]. Geometry optimizations were performed at the M06-2X[2]/Def2-TZVP[3, 4] level of theory with D3zero[5] dispersion correction. The one-electron energies were obtained at the B3PW91[6, 7]/Def2-TZVPP level of theory. DFT simulations of the periodic structures were conducted by CP2K[8] (version 2025.1). Geometry optimization was performed using the PBE[9] functional with DFT-D3[5] dispersion correction. The Brillouin zone was sampled at the gamma point, and the plane wave cutoff energy was 500 Ry. The Multiwfn[10] and VMD[11] codes were used for the ESP, integral overlap analysis, and visualization.

Materials

Dimethylformamide (DMF, anhydrous 99.8%), dimethyl sulfoxide (DMSO, anhydrous 99.7%), isopropyl alcohol (IPA, anhydrous 99.5%), ethyl acetate (EA, anhydrous 99.5%), rubidium iodide (RbI, 99.9%), and SnF_2 (99%) were purchased from J&K Scientific. Lead bromide ($PbBr_2$), lead iodide (PbI_2), [4-(3,6-Dimethyl-9H-carbazol-9-yl)butyl]phosphonic acid (Me-4PACz), [2-(3,6-Dimethoxy-9H-carbazol-9-yl)ethyl] phosphonic acid (MeO-2PACz), [4-(7H-Dibenzo[c,g]carbazol-7-yl)butyl]phosphonic acid (4PADCB), ammonium thiocyanate (NH_4SCN), p-phenylenediamine (PPD, >98%) and (4-Fluorophenyl)thiourea (FPT, >97%) were purchased from TCI Shanghai. Cesium iodide (CsI), propane-1,3-diammonium iodide ($PDAI_2$), ethylenediamine diiodide ($EDAI_2$), and C_{60} were purchased from Xi'an Yuri Solar. Formamidinium iodide (FAI) and SnI_2 (99.99%) were obtained from Advanced Election Technology.

Bathocuproine (BCP) was obtained from Wako Chemical. PEDOT: PSS (Clevious P VP AI 4083) was obtained from Heraeus. Toluene was obtained from Sinopharm. Tetrakis(dimethylamino)tin(IV) (TDMASn, 99.9999%) was obtained from Suzhou Yuanzhan. All materials were used as received.

Perovskite precursors

Wide-bandgap perovskite $Cs_{0.2}FA_{0.8}Pb(I_{0.61}Br_{0.37})_3$: The 1.2 M precursor was prepared by mixing CsI (0.24 mmol), FAI (0.96 mmol), $PbBr_2$ (0.67 mmol), PbI_2 (0.53 mmol), and $Pb(SCN)_2$ (2 mg) in 800 μL of DMF and 200 μL of DMSO. The precursors were dissolved at 50 °C for 2-3 h and filtered through a 0.22-μm PTFE filter before use.

Narrow-bandgap perovskite $Rb_{0.04}Cs_{0.2}FA_{0.76}Pb_{0.5}Sn_{0.5}I_3$: The 2 M precursor was prepared by mixing RbI (0.08 mmol), CsI (0.4 mmol), FAI (1.52 mmol), PbI_2 (1 mmol), SnI_2 (1 mmol), SnF_2 (0.11 mmol), NH_4SCN (0.045 mmol), PEACl (0.008 mmol) and PPD (0.07 mmol) into 700 μL of DMF and 300 μL of DMSO. The precursors were dissolved at room temperature and filtered through a 0.22-μm PTFE filter before use.

Fabrication of Single-junction WBG PSCs

Patterned FTO substrates (AGC, 2.2 mm, 6-8 Ω/□) were sequentially cleaned using detergent, deionized water, acetone, and IPA under ultrasonication for 15 mins. After being dried by nitrogen flow, the substrates were treated with ultraviolet ozone for 15 min. NiO layer was deposited on the FTO substrate by spray pyrolysis. Nickel acetylacetonate (2 mmol) was dissolved in acetonitrile (38 ml) and ethanol (2 ml). The solution was sprayed by an air nozzle using clean dry air as carrier gas onto the FTO substrates, which were previously heated to 400 °C on a hot plate. The substrates were kept at 400 °C for 20 min and then cooled down to room temperature before moving

into glovebox. Me-4PACz (0.5 mg/ml in IPA) was spin-coated at 3000 rpm for 25 s, followed by annealing at 100 °C for 10 min. After cooling down, FPT (0.5 mg/ml in IPA) was spin-coated at 3000 rpm for 25 s, followed by annealing at 100 °C for 5 min. The perovskite precursor was spin-coated with a two-step procedure. The first step was at 2000 rpm for 10 s with an acceleration of 200 rpm s^{-1}; the second step was at 4000 rpm for 40 s with an acceleration of 1000 rpm s^{-1}. Ethyl acetate (300 μL) was dropped 20 s before the end of the spin, followed by annealing at 100 °C for 15 min. After cooling, $PDAI_2$ (1 mg/mL in IPA) was dropped onto the perovskite films and spin-coated at 4000 rpm for 25 s, followed by annealing at 100 °C for 5 min. Then, 20 nm C_{60} was deposited at the rate of 0.2 Å/s in a vacuum chamber (< 3×10^{-4} Pa). Then the samples were transferred to the atomic layer deposition system (T-ALD, KE-MICRO). A SnO_2 layer (~15 nm) was deposited at 85 °C by 130 cycles of the following: 0.35 s TDMASn pulse, 8 s purge, 0.1 s deionized water pulse, and 8 s purge. Finally, Cu (100 nm) was thermally evaporated in a vacuum chamber (< 3×10^{-4} Pa).

Fabrication of all-perovskite tandem solar cells

The WBG sub-cells were fabricated following the procedure described above. After ALD-SnO_2 deposition, an IZO recombination layer (~120 nm) was deposited at room temperature by radio-frequency magnetron sputtering (70 W) using a 4-inch IZO target in pure argon (0.3 Pa). PEDOT: PSS diluted with IPA (1:2 volume ratio) was spin-coated onto the as-prepared IZO layer at 4000 rpm for 30 s, followed by annealing at 120 ℃ for 10 min in air, and then moved into a N_2-filled glovebox. The Sn-Pb perovskite films were deposited with a two-step spin-coating procedure: 1000 rpm for 10 s with an acceleration of 200 rpm s^{-1}; and 4000 rpm for 40 s with an acceleration of 1000 rpm s^{-1}. Ethyl acetate (400 μL) was dropped on the substrate at 20 s before the end

of the procedure. Then 0.5 mg/ml $EDAI_2$ solution in mixed IPA/toluene (2:1 volume ratio) was applied onto the cooled perovskite films and spin-coated at 4000 rpm for 25 s, followed by annealing at 100 ℃ for 5 min. Then the substrates were transferred to the evaporation system, and C_{60} (15 nm), BCP (8 nm), and Cu (100 nm) were deposited sequentially in a vacuum chamber ($< 3 \times 10^{-4}$ Pa).

Film Characterizations

GIWAXS measurements were performed at the BL20U2 beamline in Shanghai Synchrotron Radiation Facility using 10 KeV X-rays. The grazing-incidence angle was 1° and the exposure time was 20 s. The X-ray diffraction (XRD) was conducted using an X-ray diffractometer (ARL Equinox 3500) with Cu Kα radiation at a scan speed of 2°/min. Fourier transform infrared spectroscopy was performed on a Nicolet 6700 spectrophotometer. The SEM images of perovskite films and devices were collected using a Gemini 300 instrument. KPFM measurements were conducted on the FastScan Bio (Bruker). X-ray photoelectron spectroscopy measurements were performed on an ESCALAB Xi+ spectrometer using an Al Ka X-ray source. Ultraviolet photoelectron spectroscopy (UPS) spectra were measured with a He Iα photon source. The binding energy scale was calibrated using a clean gold film. Photoluminescence (PL) spectra and time-resolved PL spectra were recorded by a steady-state transient fluorescence spectrometer (FLS1000). PL peak energy mappings were probed using a Raman image-scanning electron microscope (RISE-MAGNA). Absorption spectra were recorded using a UV-vis-NIR spectrometer (PerkinElmer Lambda 750S). Femtosecond transient absorption spectroscopy was conducted on Femto/Nano-TA100 (TIME-TECH SPECTRA). Contact angle measurements were carried out on a DSA100 instrument.

Device Characterizations

The current density-voltage (*J-V*) characteristics of the perovskite solar cells were measured with a Keithley 2400 source meter under simulated AM1.5G one-sun illumination provided by a dual light source simulator (WXS-90S-L2, Wacom), calibrated by a Si-reference cell (91150-KG5). For the single-junction perovskite solar cells, the *J-V* curves were acquired via reverse scan (1.35 V to -0.1 V) and forward scan (0.1 V to 1.35 V), with a voltage step of 10 mV and a delay time of 10 ms. For the all-perovskite tandem solar cells, *J-V* curves were obtained using reverse scan (2.2 V to -0.1 V) and forward scan (-0.1 V to 2.2 V), with the voltage step of 10 mV and delay time of 10 ms. The active area of the devices was defined by a black metal mask. The transient photocurrent measurements were conducted on a characterization platform for solar cells (PAIOS, Fluxim). External quantum efficiency was obtained using monochromatic incident light of 1×10^{16} photons cm^{-2} in direct current mode (CEP-2000BX, Bunko-Keiki). Space charge limited current, dark *J-V* curves, and Mott-Schottky curves were collected on an electrochemical analysis instrument (Zahner, Germany).

For the thermal stability measurement, the unencapsulated devices were placed on a heating plate at 85 °C in the N_2-filled glovebox (H_2O, <0.01 ppm; O_2, <0.01 ppm). All the devices are cooled down before each measurement. Device encapsulation was conducted using glass-to-glass sealing with a caved glass cover and epoxy encapsulant (Three Bond). For maximum power point tracking, the encapsulated device was operated in ambient air (30-40% RH, 20-30 ℃) under simulated one-sun illumination (Xenon lamp). No UV filter was applied during operation

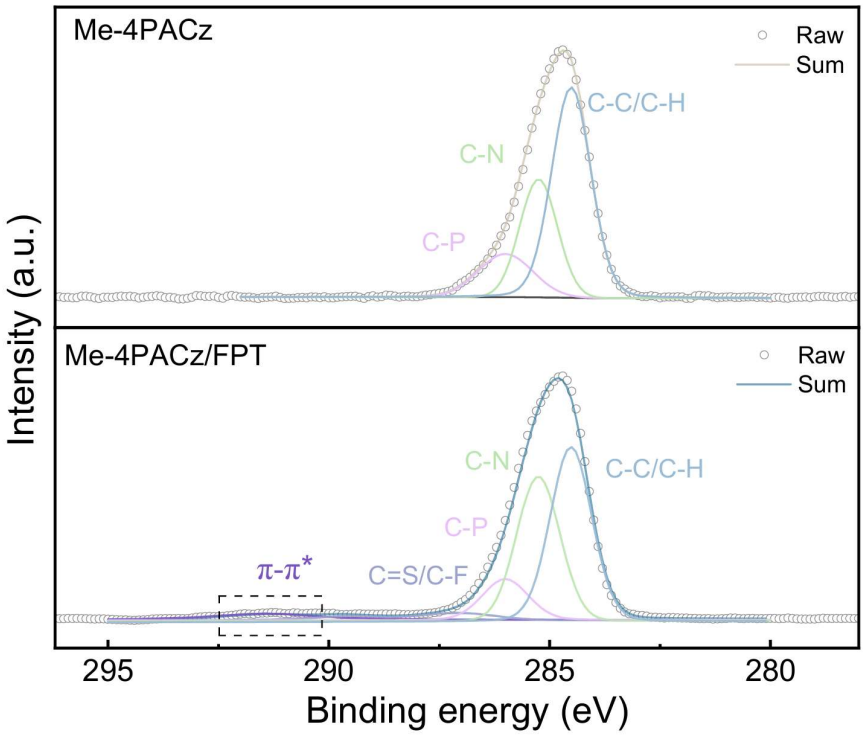

Figure S1. XPS C 1s core-level spectra of Me-4PACz and Me-4PACz/FPT hybrid.

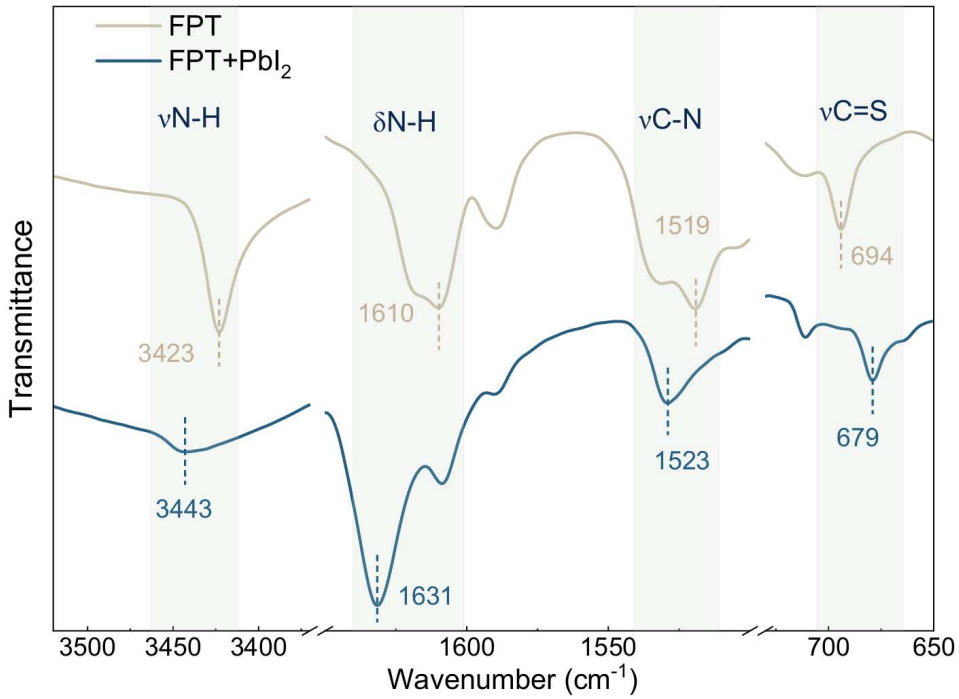

Figure S2. FTIR spectra of FPT and FPT+PbI_2 mixture.

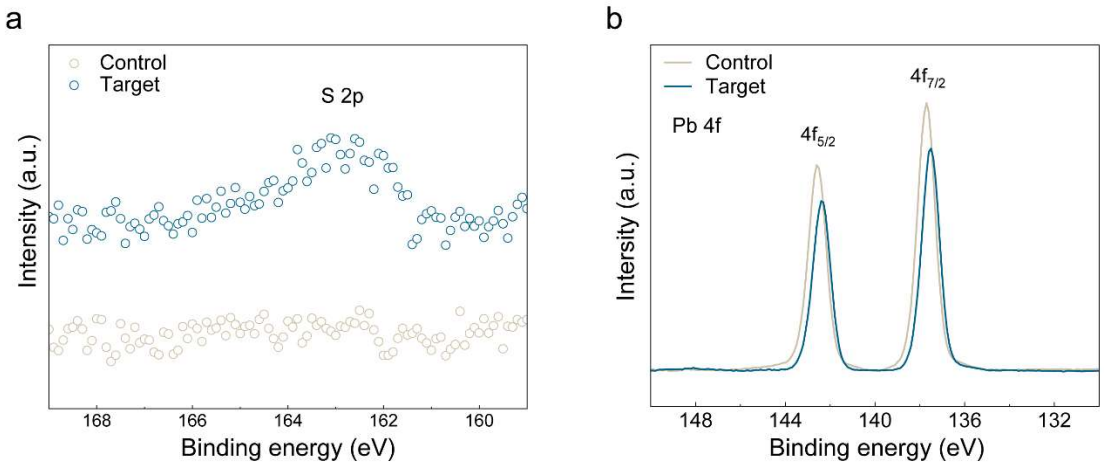

Figure S3. XPS spectra collected on the buried surface of the perovskite films deposited on Me-4PACz (control) and Me-4PACz/FPT (target) substrates. (a) S 2p core-level; (b) Pb 4f core-level.

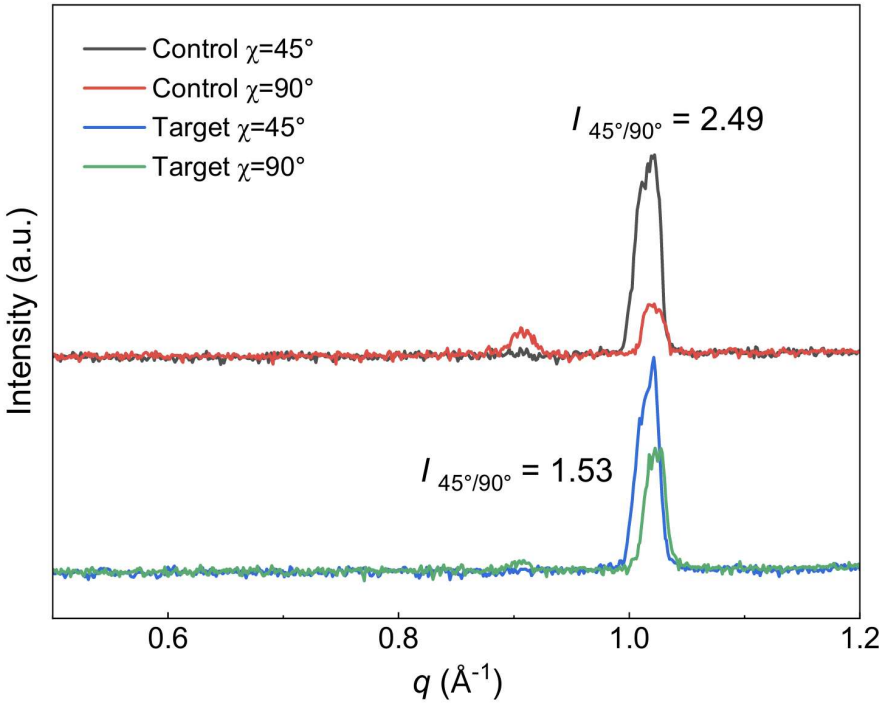

Figure S4. Linecut intensity profiles of the GIWAXS patterns at 45° and 90° azimuthal angles.

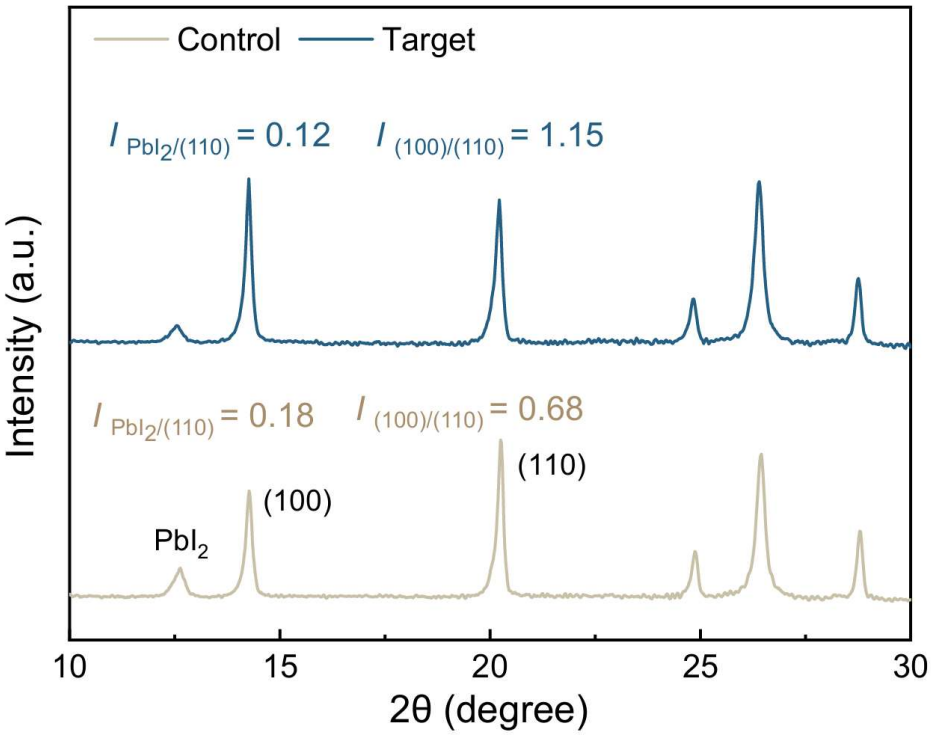

Figure S5. XRD patterns of the perovskite films deposited on Me-4PACz and Me-4PACz/FPT.

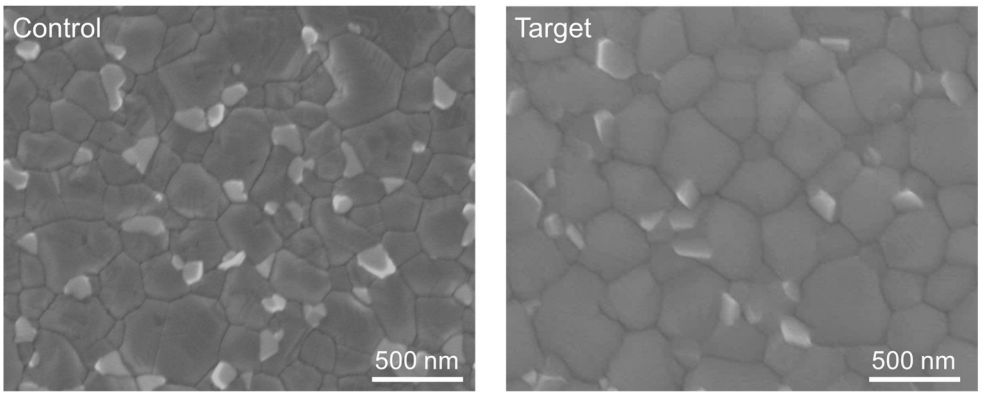

Figure S6. SEM images of top surface of the perovskite films.

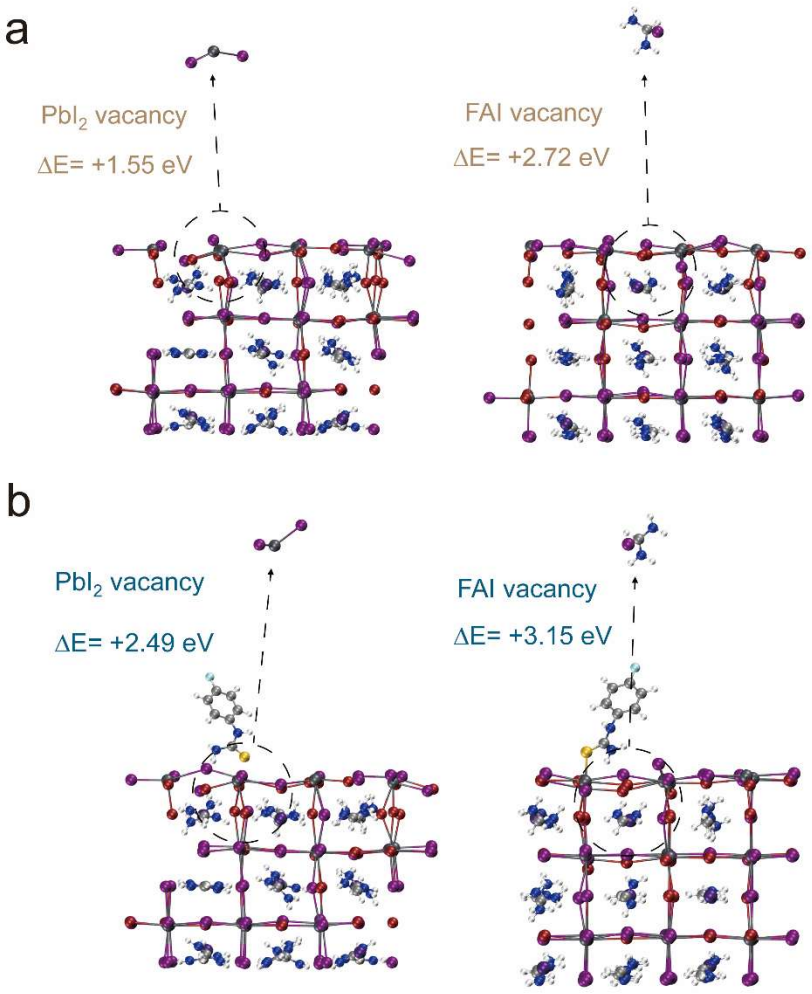

Figure S7. Formation energy of the neutral PbI_2 and FAI vacancies on the Pb-I/Br-terminated grain surface (a) without and (b) with FPT.

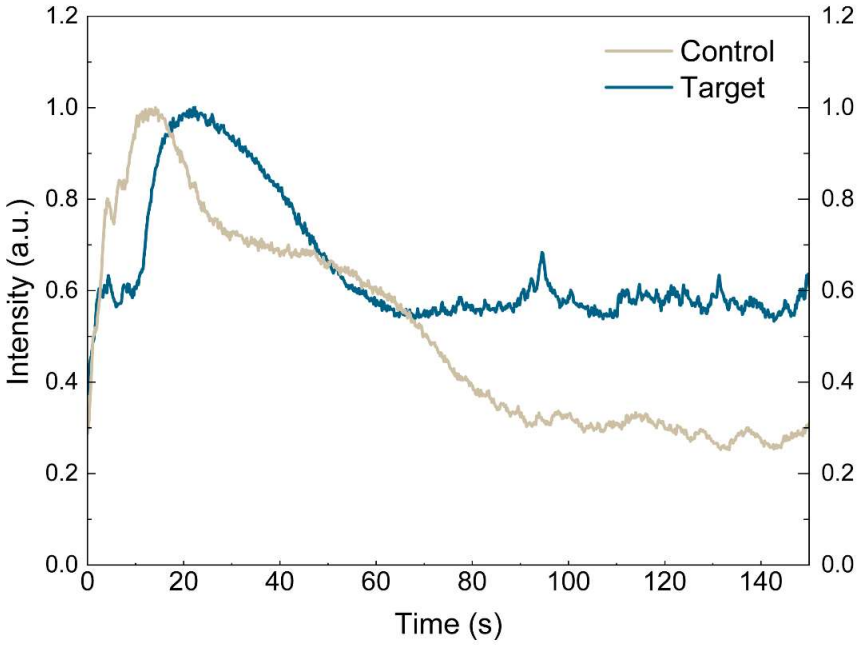

Figure S8. Evolution of emission intensity (probed at 709 nm) of the perovskite films during annealing, normalized at their maxima.

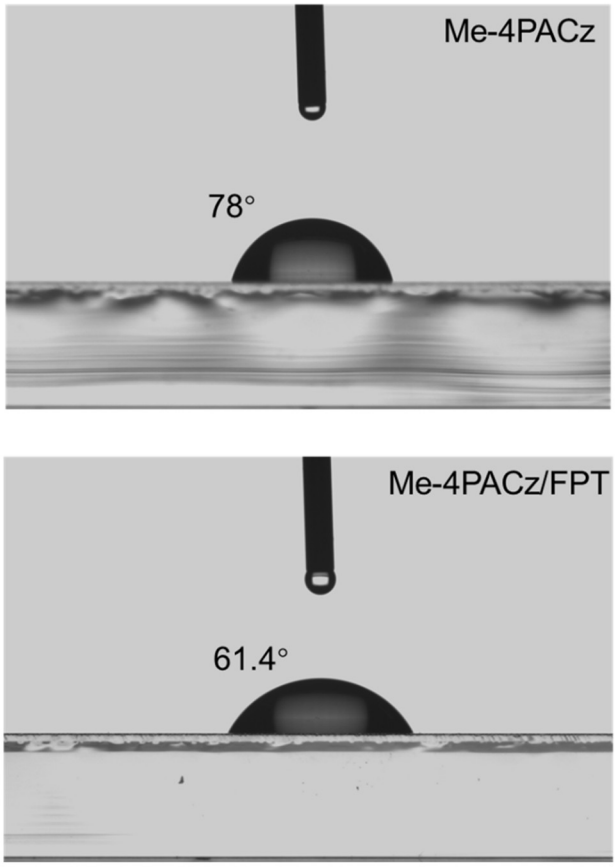

Figure S9. Contact angle images of perovskite precursor on Me-4PACz and Me-4PACz/FPT substrates.

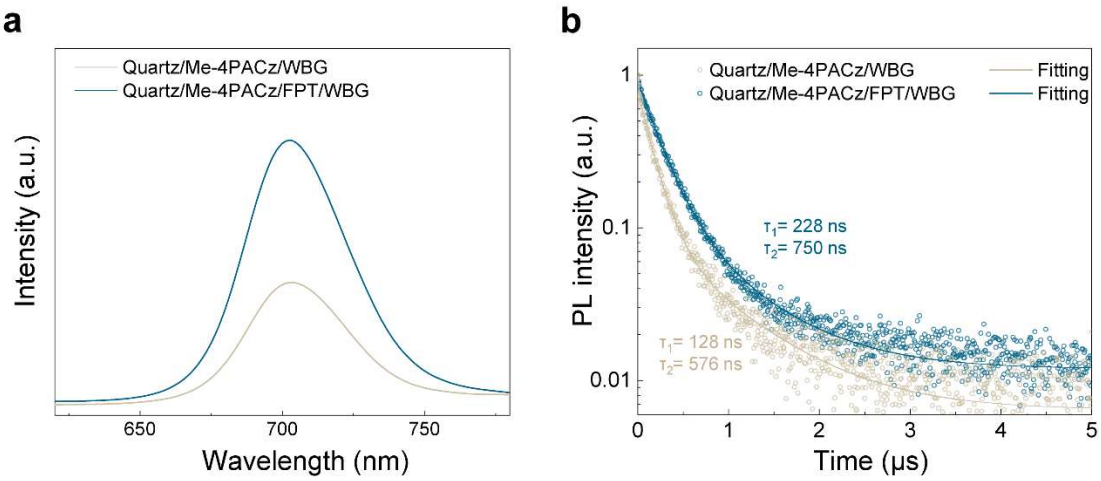

Figure S10. (a) PL spectra and (b) time-resolved PL decay of the perovskite films deposited on quartz/Me-4PACz and quartz/Me-4PACz/FPT. The TRPL fitting details are shown in Table S1.

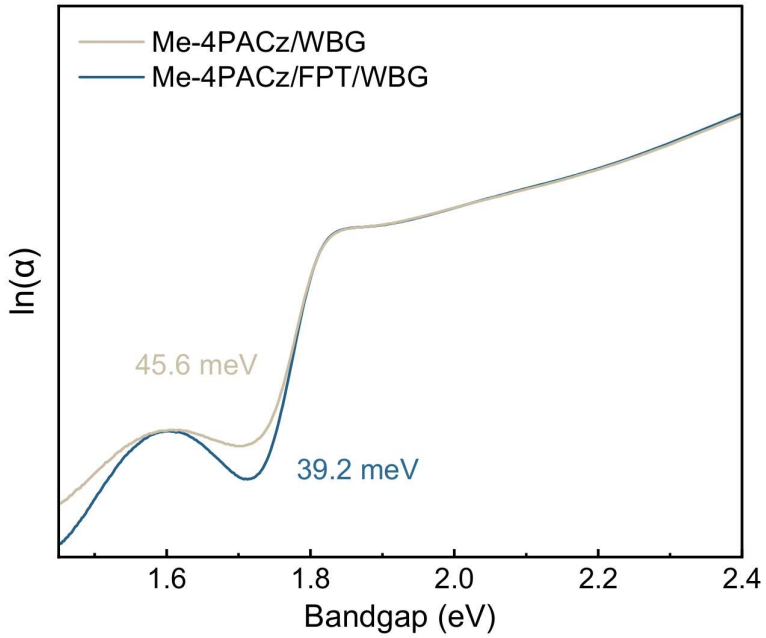

Figure S11. Urbach energies of the perovskite films deposited on quartz/Me-4PACz and quartz/Me-4PACz/FPT, derived from the absorption curves.

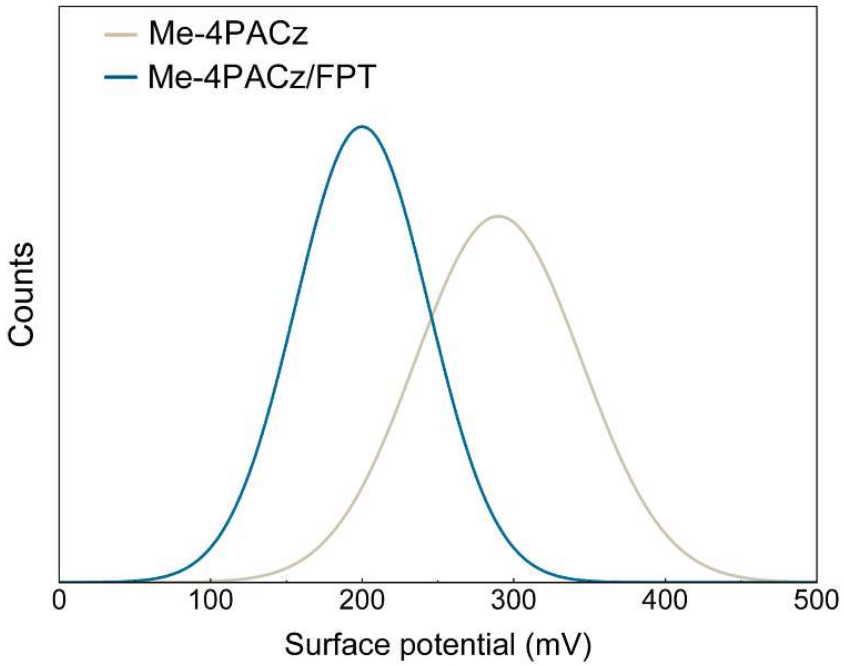

Figure S12. Statistical distribution of the surface potential values of Me-4PACz and Me-4PACz/FPT hybrid.

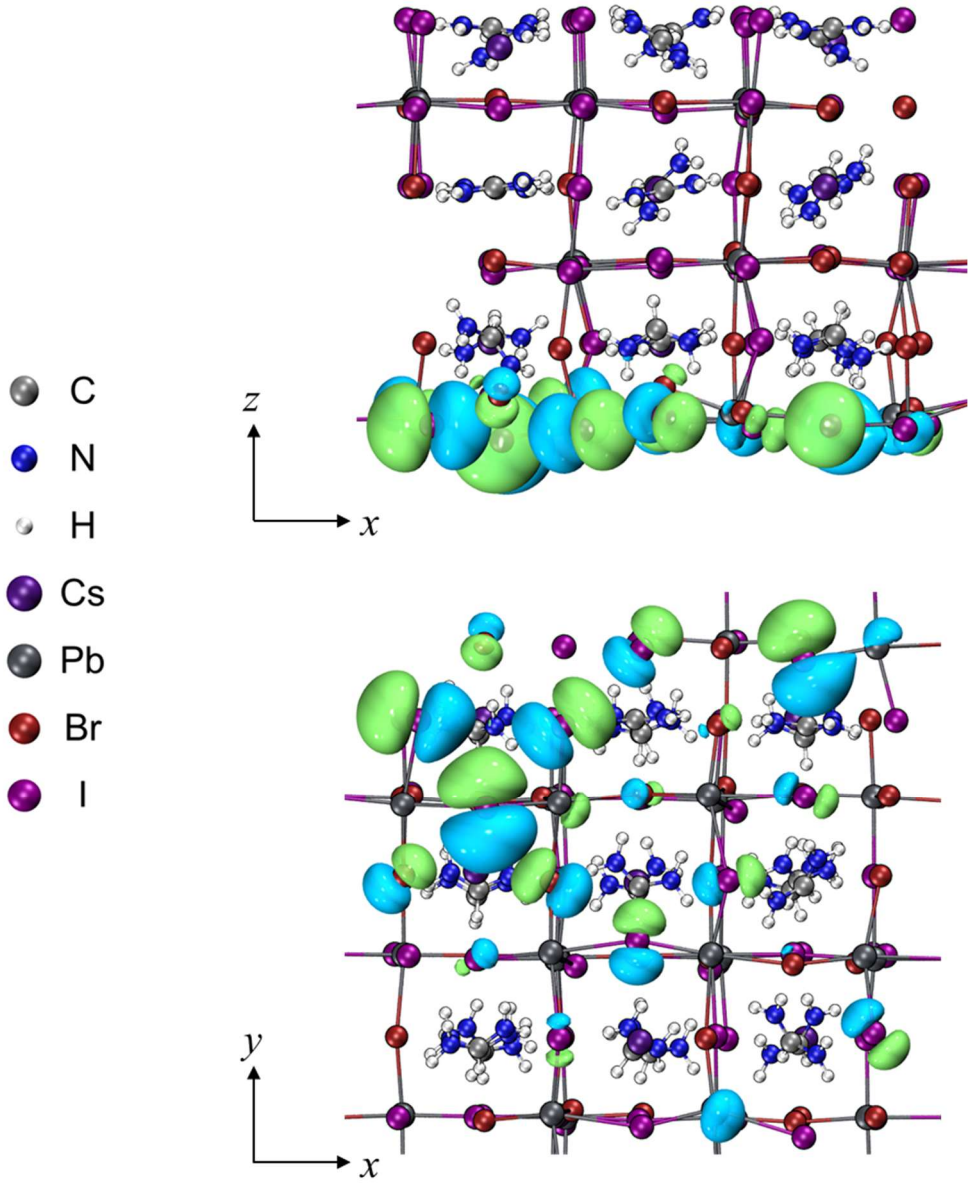

Figure S13. Wavefunction iso-surfaces of the VBM orbital of WBG perovskite. Green, positive value; blue, negative value.

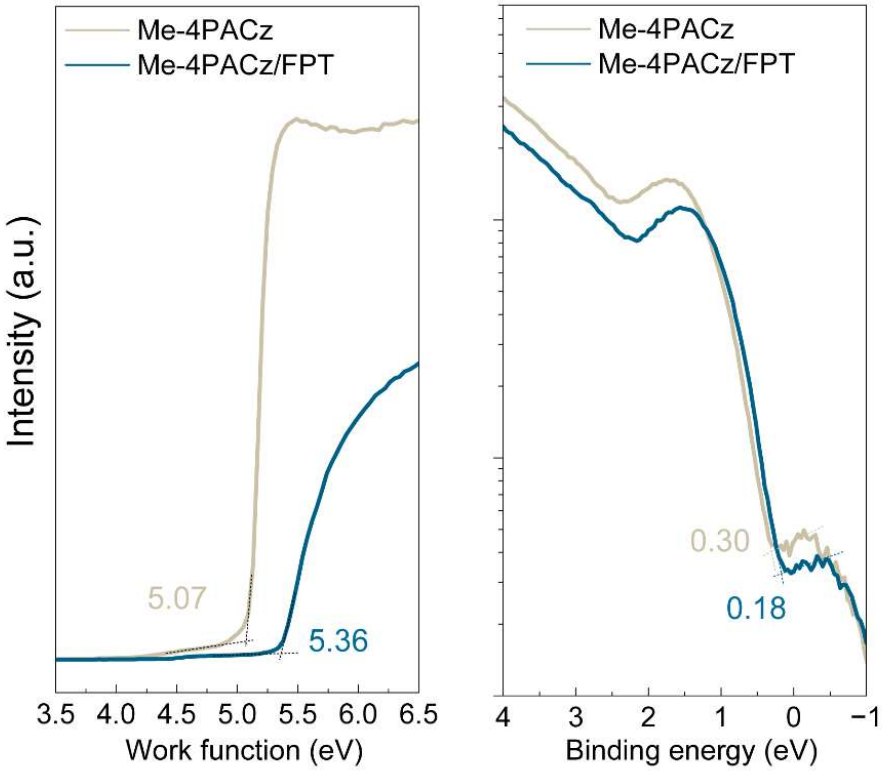

Figure S14. UPS spectra of Me-4PACz and Me-4PACz/FPT hybrid.

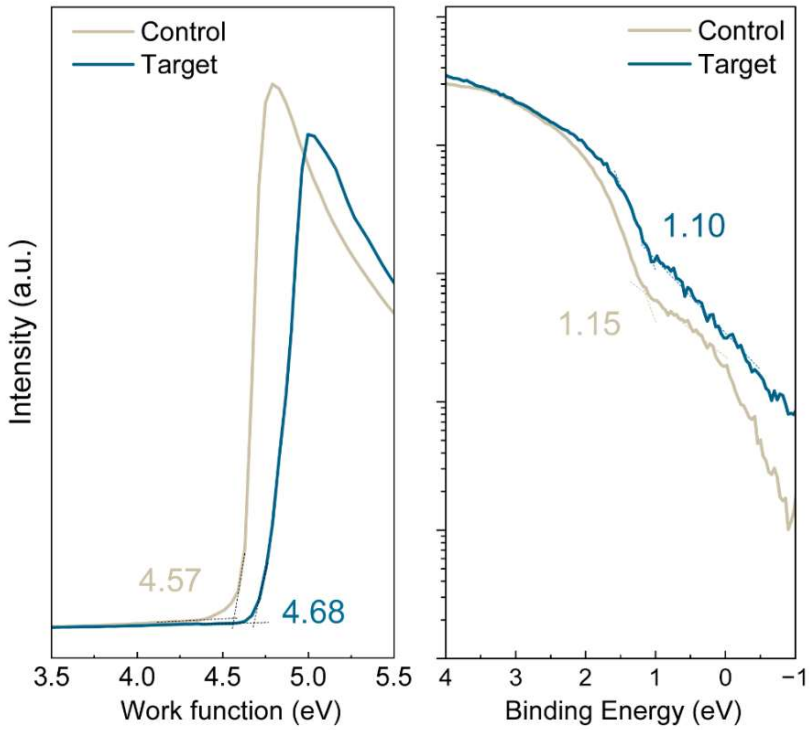

Figure S15. UPS spectra collected on the buried surface of the perovskite films deposited on Me-4PACz (control) and Me-4PACz/FPT (target).

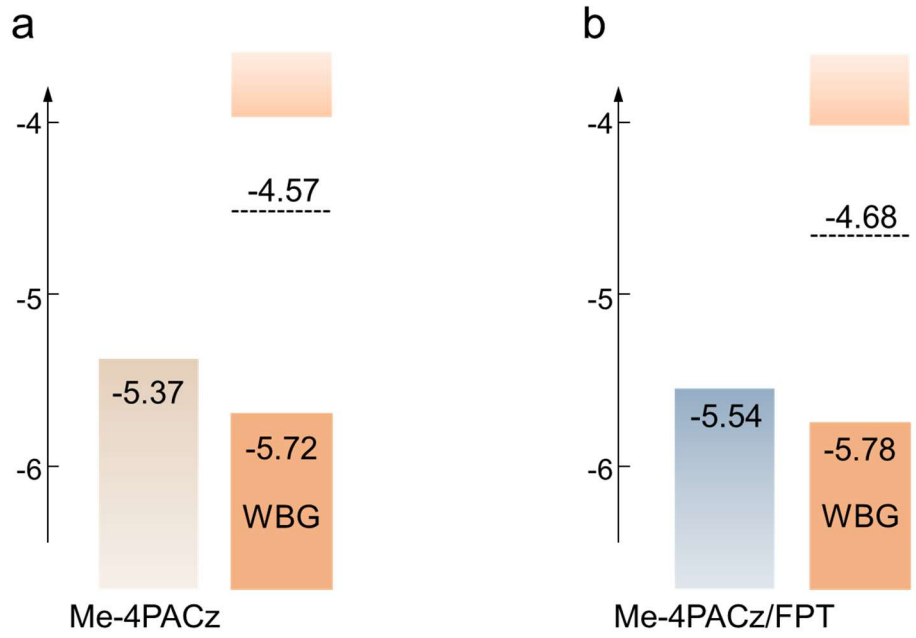

Figure S16. Energy level alignment at the hole collecting heterointerface of (a) control and (b) target devices.

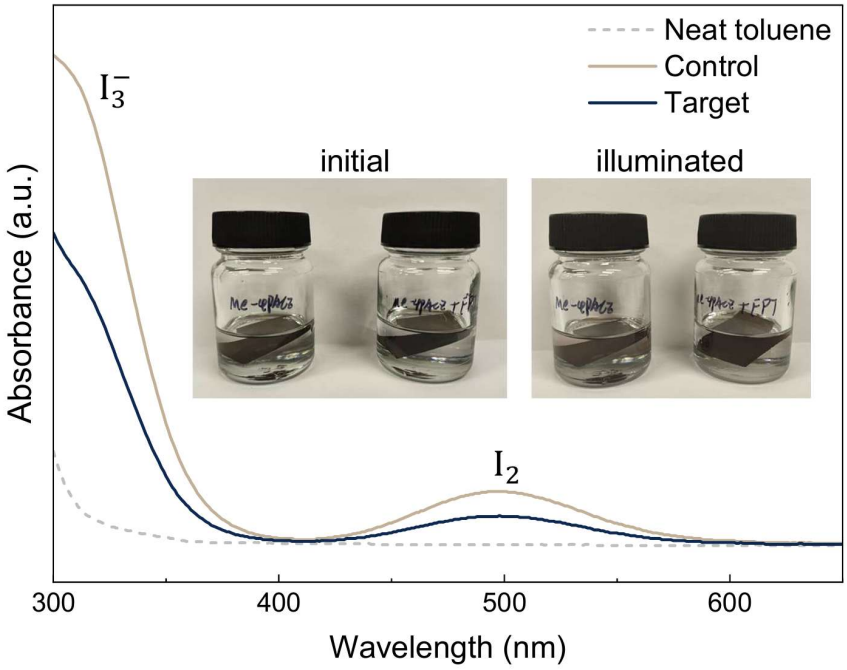

Figure S17. Absorption curves of the toluene solutions containing the perovskite films. Inset, photos of the toluene solution before and after illumination.

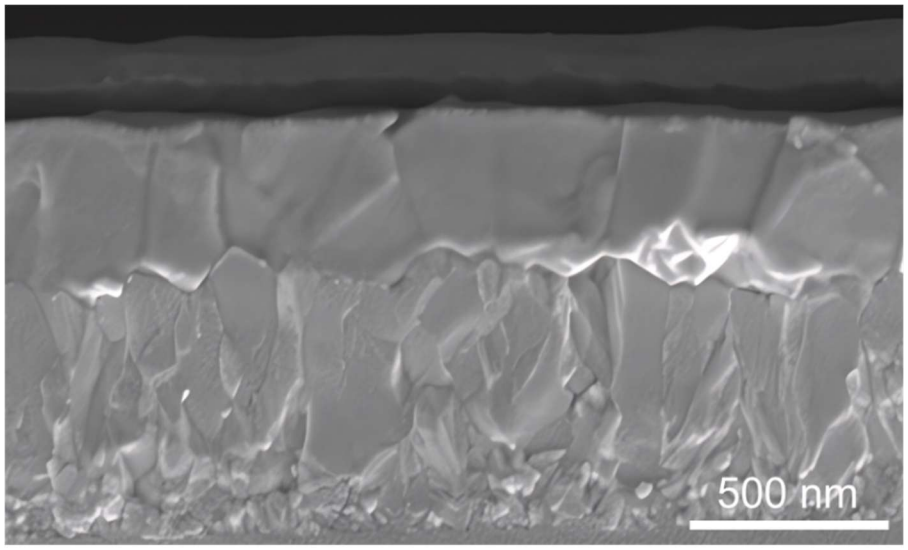

Figure S18. Cross-sectional SEM image of a single-junction WBG PSC.

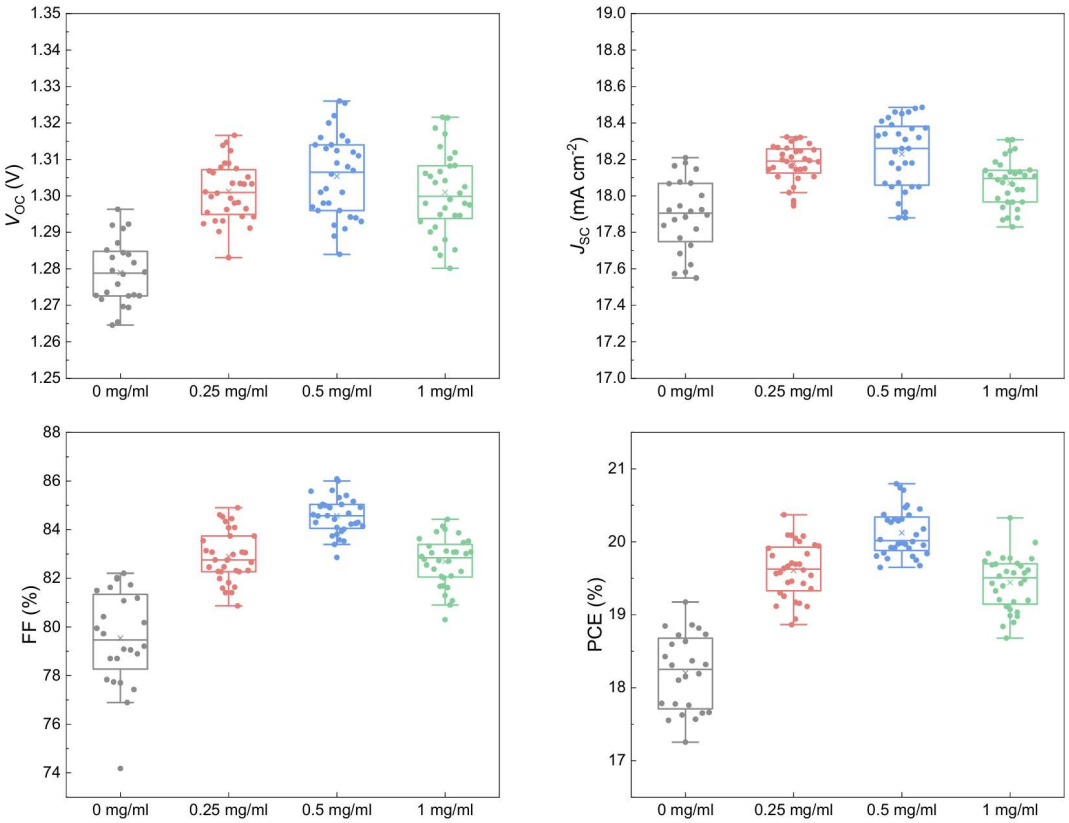

Figure S19. Photovoltaic parameters statistics of the single-junction WBG PSCs with different FPT concentrations, measured by reverse scan. Center line, median; cross mark, mean; box range, 25/75 percentiles; whiskers, the outermost outliers within 1.5 × interquartile range.

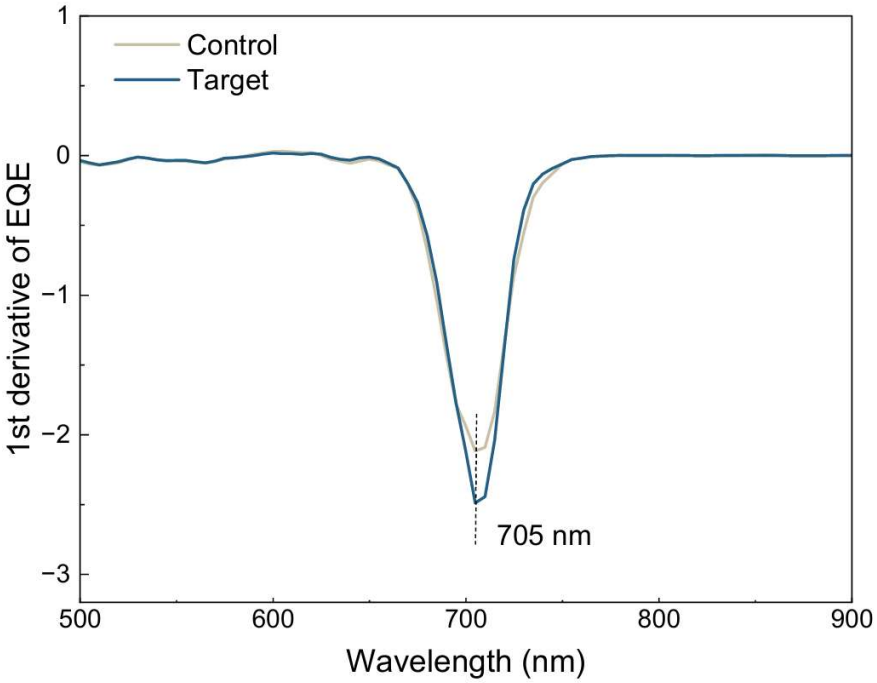

Figure S20. The first derivatives of the EQE curves.

福建省计量科学研究院
FUJIAN METROLOGY INSTITUTE
（国家光伏产业计量测试中心）
National PV Industry Measurement and Testing Center

中国认可 国际互认 检测 TESTING CNAS L0131

检 测 报 告
Test Report

报告编号： 25Q3-00100
Report No.

客户信息 Name of Custome	上海交通大学/Shanghai Jiao Tong University
联络信息 Contact Information	上海市闵行区东川路800号/800 Dongchuan Road. Minhang District, Shanghai, China
物品名称 Name of items	钙钛矿太阳能电池/perovskite solar cell(IV)
型号/规格 Type /Specification	25mm × 25mm
物品编号 Ittems No	L2-2
制造厂商 Manufacturer	上海交通大学/Shanghai Jiao Tong University
物品接收日期 Items Receipt Date	2025-01-13
检测日期 Test Date	2025-01-20

批准人： 黎健生 Approved by

（盖章处） Stamp

核验员： 何翔 Checked by

检测员： 陈彩云 Test by

发布日期： 2025 年 01 月 20 日
Date of Report Year Month Day

扫一扫 查真伪

本院/本中心地址：福州市屏东路9-3号 Address：9-3 Pingdong Road,Fuzhou,China
电话：0591-87845050 Telephone
传真：0591-87808417 Fax
邮编：350003 Post Code
网址：www.fjjl.net Web Site
咨询电话：0591-87845050 Inquire line
投诉电话：0591-87823025 Complaint Tel

报告编号：25Q3-00100
Report No.

1. 检测机构说明：
Testing institutions that

本院为国家法定计量检定机构，国家光伏产业计量测试中心依托本院检测技术开展检测。本院/本中心质量管理体系符合GB/T 27025（ISO/IEC 17025，IDT）标准要求。

The institute is a national legal metrological institution. National PV Industry Measurement and Testing Center carrys out testing relying on the institute's testing technology. The Center's quality management system meets the requirements of GB/T 27025（ISO/IEC 17025，IDT）standard.

2. 本次检测所依据的检测方法（代号及名称）：
Reference documents for the test (code,name)

SJ/T 11630—2016 太阳能电池用硅片几何尺寸测试方法;IEC 60904-1-2020 光伏器件-第一部分：光伏电流-电压特性的测量

3. 本次检测所使用的主要测量仪器:
Measurement standards used in this test

仪器名称 Name	仪器编号 Number	测量范围 Measuring Range	不确定度/或准确度等级/或最大允许误差 Uncertainty or Accuracy Class or Maximum Permissible Error	溯源机构名称/证书编号 Name of traceability institution/Certificate No.	有效期限 Due date
WPVS单晶硅标准电池	015-2014	（300～1200）nm	U_{rel}=1.3%（k=2）	中国计量院 GXgf2023-01245	2025-03-29
源表	10807C00878-2	电流：10μA~1A；电压：20mV~20V	测量：DCV:U_{rel}=0.05%，k=2；DCI:U_{rel}=0.05%，k=2 输出：DCV:U_{rel}=0.05%，k=2；DCI:U_{rel}=0.05%，k=2	福建计量院24D2-01917	2025-04-17
太阳模拟器	2014-017	（300~1200）nm;（300~1200）W/m^2	光谱匹配度（300~360）nm：U_{rel}=8.0%（k=2）;（360~1200）nm：U_{rel}=6.2%（k=2）；辐照度比（辐照度不均匀度、辐照度时间不稳定度）：U_{rel}=1.2%（k=2）	福建计量院24Q2-00981	2025-06-16
数字温度计	15-B	（15～65）℃	U=0.1 ℃（k=2）	福建计量院24B2-05374	2025-06-19
自动影像测量仪	11656	X轴：（0～195）mm；Y轴：（0～195）mm	U=2 μm（k=2）	福建计量院24A2-09430	2025-07-23
/	/	/	/	/	/

4. 检测地点及环境条件
Location and environmental condition for the test

地点：本院闽侯科研基地4号楼108室/Room 108, Building 4, MinHou Scientific Research Base
Location

温度：24.7 ℃ 相对湿度：38 % 其它：/
Temperature Relative Humidity Others

5. 备注：/
Note

本报告提供的结果仅对本次被检的物品有效。
The data are valid only for the instrument(s) under testing.

检测报告续页专用
Continued page of test report

检测结果/说明：
Results of Test and additional explanation.

1. 标准测试条件 Standard Test Condition (STC)：

总辐照度 Total Irradiance：1000 W/m^2
被测电池温度 Temperature：25.0 °C
光谱分布 Spectral Distribution：AM1.5G

2.STC条件下测量数据 Measurement Data and I-V/P-V Curves under STC

正扫 Forward Scan

I_{sc} (mA)	V_{oc}(V)	I_{MPP}(mA)	V_{MPP}(V)	P_{MPP} (mW)	FF(%)	A (cm^2)
1.766	1.301	1.648	1.147	1.890	82.26	0.0948

反扫 Reverse Scan

I_{sc} (mA)	V_{oc}(V)	I_{MPP}(mA)	V_{MPP}(V)	P_{MPP} (mW)	FF(%)	A (cm^2)
1.767	1.305	1.682	1.147	1.929	83.65	0.0948

失配因子 Mismatch factor: 1.004

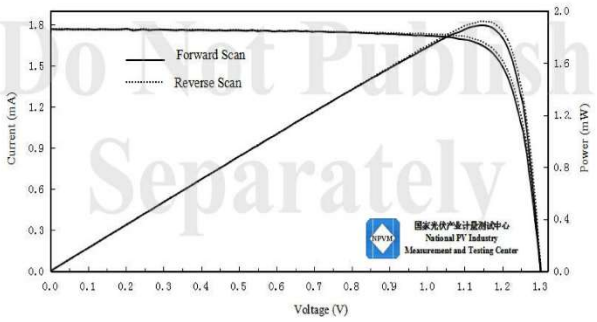

图1 STC下电流-电压特性曲线和功率-电压特性曲线
Figure 1. I-V and P-V characteristic curves of the measured sample under STC

检测结果/说明：
Results of Test and additional explanation.

3.STC条件下最大功率稳态输出的测量数据及曲线Measurement Data and Curves for MPPT under STC

η (%)	19.57
P_{MPP} (mW)	1.855
I_{MPP} (mA)	1.624
V_{MPP} (V)	1.142

说明：上表为300秒测试过程中最后 30 秒内 STC 条件下的最大功率稳态输出平均测试数据
Note: Measurement data for MPPT under STC in the above table was the mean value acquired during the final 30 seconds of the 300 seconds test

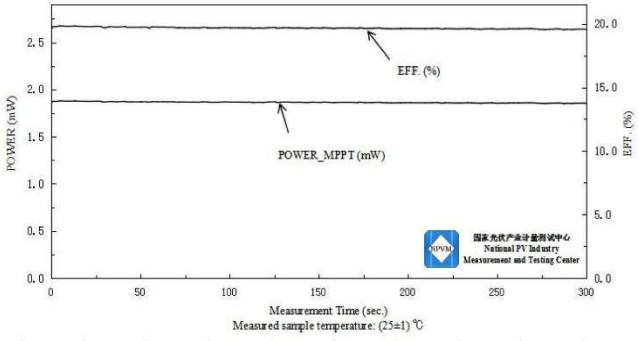

图2 被测样品最大功率稳态输出的功率-效率曲线
Figure 2. Measurement curves of the measured sample for MPPT

检测结果/说明：
Results of Test and additional explanation.

4.Pictures of the Measured Sample

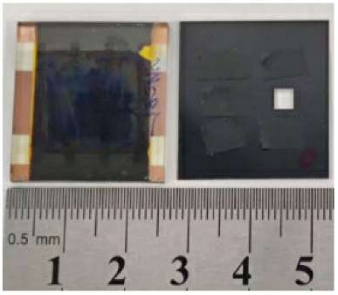

图3 被测样品的正面图像及测试中使用的掩膜板
Figure 3. Mask used during test and obverse side of the measured sample

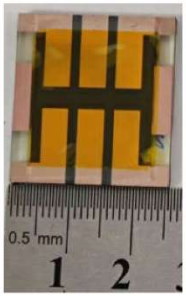

图4 被测样品的反面图像
Figure 4. Reverse side of the measured sample

测量结果的不确定度为/Uncertainty of measurement results:
短路电流/Short-Circuit Current: U_{rel}=1.8 % (k=2); 开路电压/Open-Circuit Voltage: U_{rel}=1.0 % (k
最大功率/Maximum Power: U_{rel}=2.2 % (k=2); 转换效率/Efficiency: U_{rel}=2.2 % (k=2);
填充因子/Fill Factor: U_{rel}=3.2 % (k=2).
说明：该报告中的面积为限定辐照面积。
Explanation：The measured area refers to designated illuminated area.

福建省计量科学研究院
FUJIAN METROLOGY INSTITUTE
（国家光伏产业计量测试中心）
National PV Industry Measurement and Testing Center

报告编号： 25Q3-00100
Report No.

检测结果/说明：
Results of Test and additional explanation.

Testing Method (Code and Name) for This Test
IEC 60904-1: 2020 Photovoltaic devices- Part 1: Measurement of photovoltaic current-voltage characteristics
SJ/T 11630-2016: Test method for geometric dimension of silicon wafers for solar cell

Measurement Standards Used in This Test

Name	Number	Measuring Range	Uncertainty or Accuracy Class or Maximum Permissible Error	Name of Traceability Institution/Certificate No.	Due Date
Source Meter	10807C00878-2	Current:10μA~1A; Voltage:20mV~20V	Measure: DCV:U_{rel}=0.05%,k=2; DCI:U_{rel}=0.05%,k=2 Output: DCV:U_{rel}=0.05%,k=2; DCI:	Fujian Metrology Institute/ 24D2-01917	2025-04-17
Solar Simulator	2014-017	(300～1200) nm; (800～1200) W/m^2	Spectral Match: (300～360) nm: U_{rel}=8.0% (k=2);(360～1200) nm: U_{rel}=6.2% (k=2);Irradiance Ratio: U_{rel}=1.2% (k=2)	Fujian Metrology Institute/ 24Q2-00981	2025-06-16
WPVS Monocrystalline Silicon Reference Cell	015-2014	(300～1200) nm	U_{rel}=1.3% (k=2)	National Institute of Metrology, China/ GXgf2023-01245	2025-03-29
Automatic Image Measuring Instrument	11656	X-axis: (0～195) mm; Y-axis: (0～195) mm	U=2 μm (k=2)	Fujian Metrology Institute/24A2-09430	2025-07-23
Digital Thermometer	15-B	(15～65)℃	U=0.1 ℃ (k=2)	Fujian Metrology Institute/24B2-05374	2025-06-19

以下空白
Blank below

检测报告续页专用
Continued page of test report

第 6 页/共 6 页
Page of Pages

Figure S21. The certified result of the 1.76 eV single-junction perovskite solar cell, measured at the National PV Industry Measurement and Testing Center. Anti-reflection coating was applied on the device. Under reverse scan, the device achieved a PCE of 20.35%, a J_{SC} of 18.64 mA cm^{-2}, a V_{OC} of 1.305 V, and an FF of 83.65%. Under forward scan, the device achieved a PCE of 19.94%, a J_{SC} of 18.63 mA cm^{-2}, a V_{OC} of 1.301 V, and an FF of 82.26%.

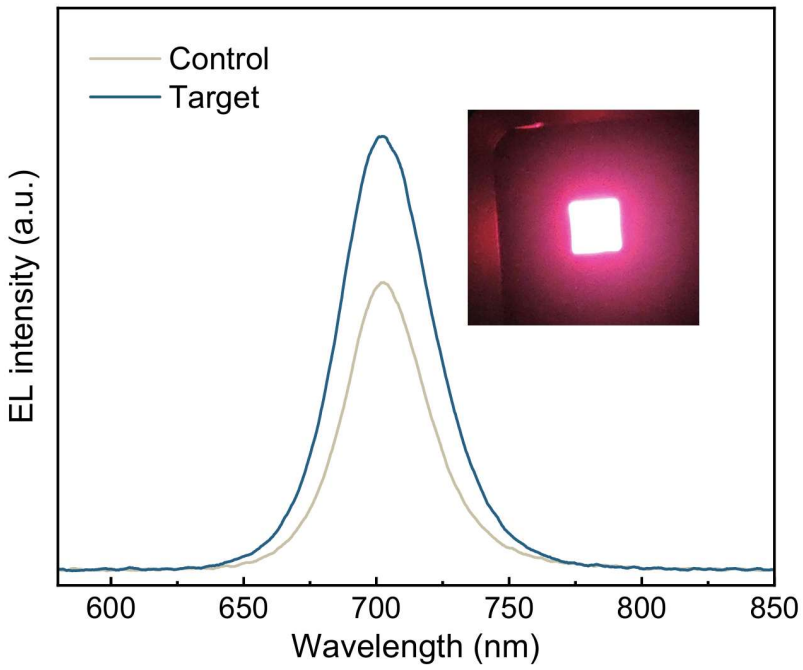

Figure S22. Electroluminescence spectra of the PSCs under 2 V bias.

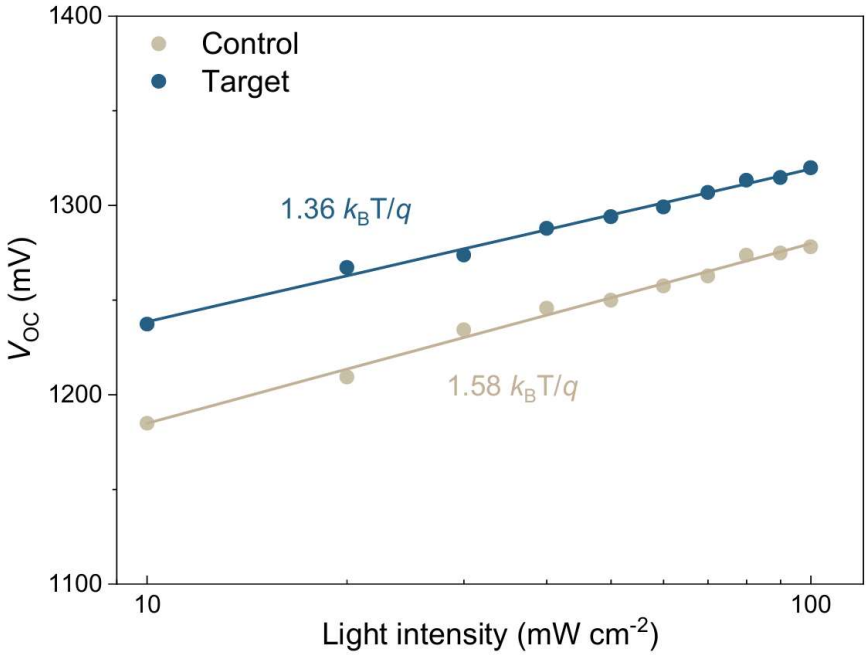

Figure S23. Light intensity dependence of the devices V_{OC}.

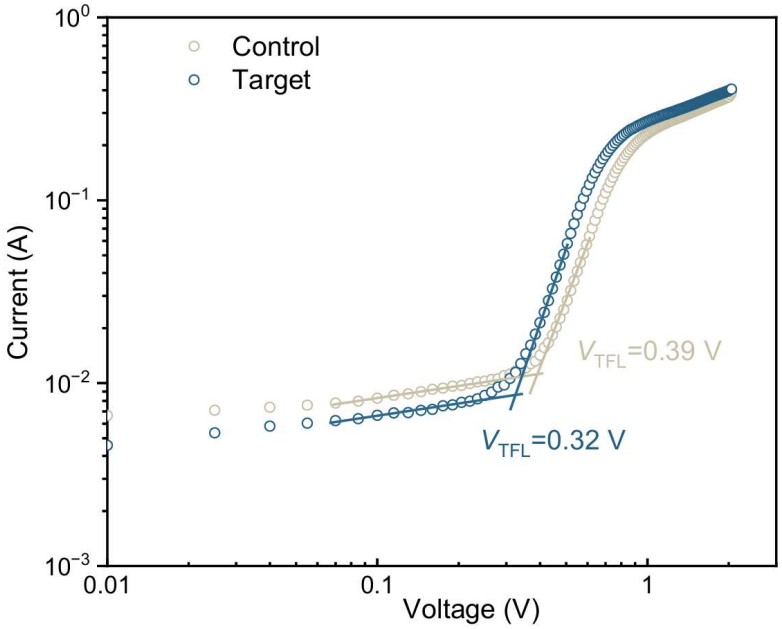

Figure S24. Logarithmic *I-V* curves of the hole-only devices FTO/NiO/SAM/WBG/Spiro-OMeTAD/Cu. Through the equation $N_d = \frac{2\varepsilon\varepsilon_0 V_{TFL}}{eL^2}$, where ε and ε_0 are the dielectric constant and vacuum permittivity, respectively, e is the unit charge, and L is the thickness of the perovskite film, trap densities of the control and target devices were determined as 7.76×10^{15} cm^{-3} and 1.06×10^{15} cm^{-3}, respectively.

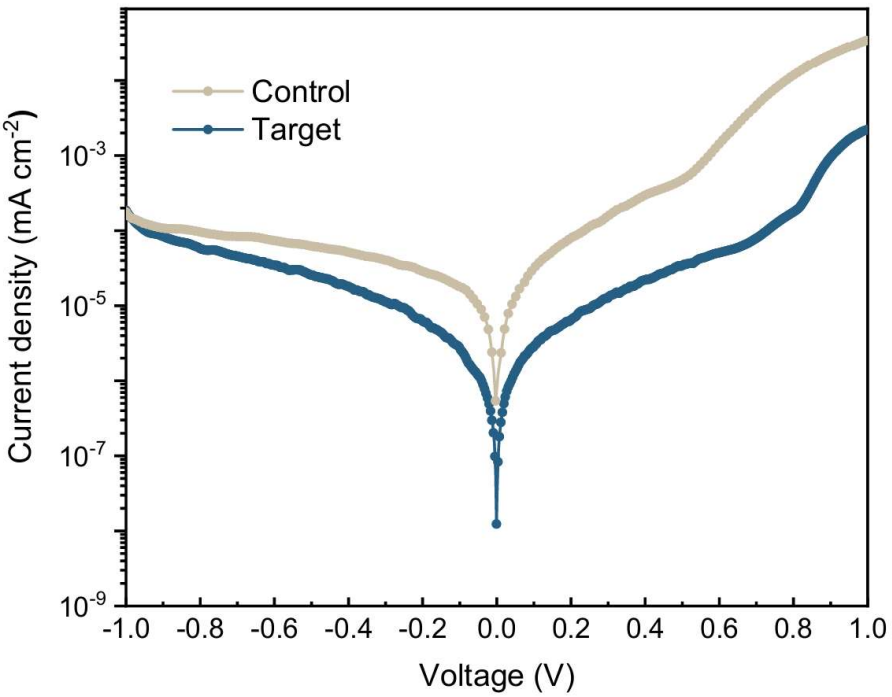

Figure S25. Dark *J-V* curves of the WBG PSCs.

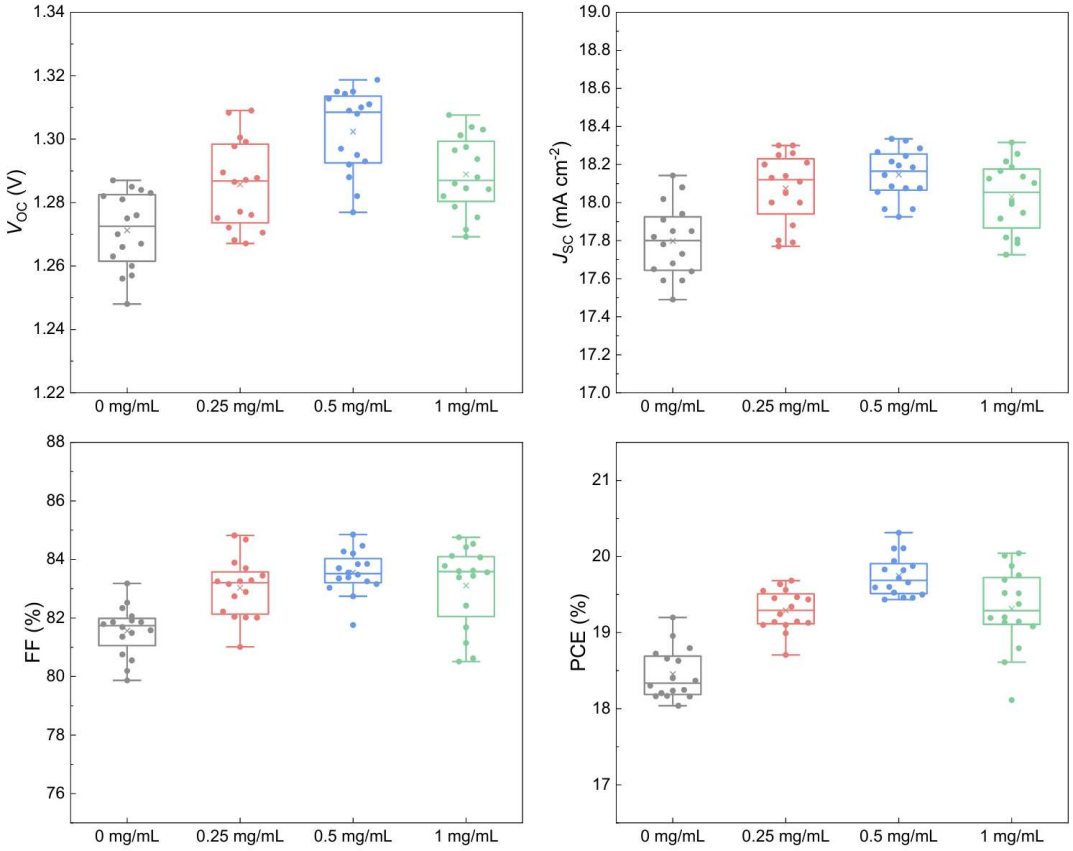

Figure S26. Photovoltaic parameters statistics of the 4PADCB-based single-junction PSCs with different FPT concentrations, measured by reverse scan. Center line, median; cross mark, mean; box range, 25/75 percentiles; whiskers, the outermost outliers within 1.5 × interquartile range.

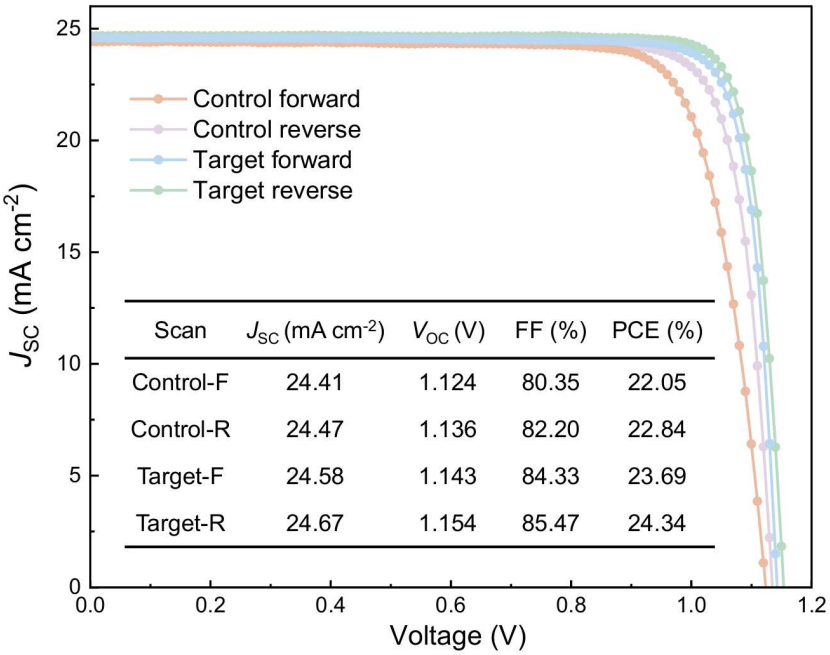

Scan	J_{SC} (mA cm^{-2})	V_{OC} (V)	FF (%)	PCE (%)
Control-F	24.41	1.124	80.35	22.05
Control-R	24.47	1.136	82.20	22.84
Target-F	24.58	1.143	84.33	23.69
Target-R	24.67	1.154	85.47	24.34

Figure S27. *J-V* curves and photovoltaic parameters of 1.53 eV PSCs with the architecture FTO/4PADCB/$Cs_{0.05}(FA_{0.98}MA_{0.02})_{0.95}Pb(I_{0.98}Br_{0.02})_3$/$EDAI_2$/$C_{60}$/BCP/Cu.

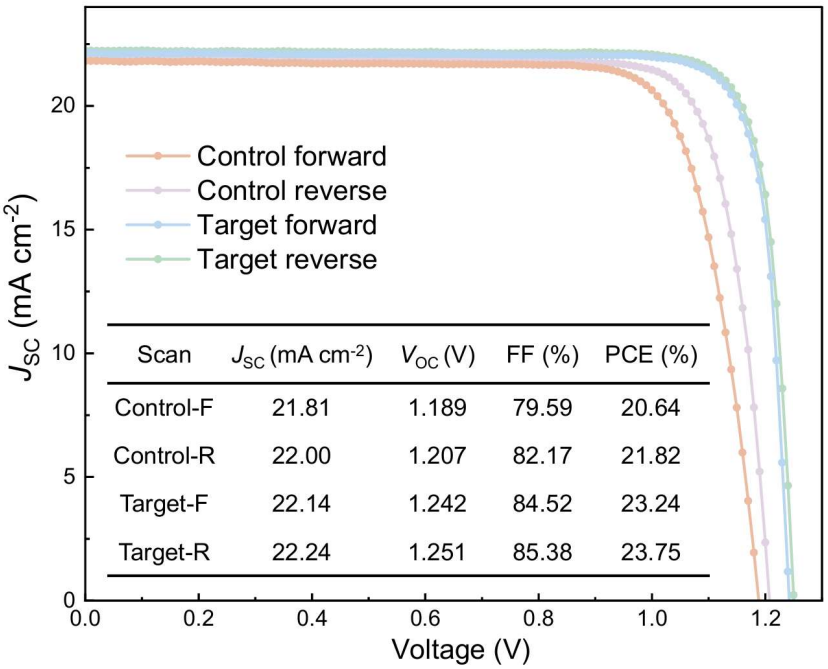

Scan	J_{SC} (mA cm^{-2})	V_{OC} (V)	FF (%)	PCE (%)
Control-F	21.81	1.189	79.59	20.64
Control-R	22.00	1.207	82.17	21.82
Target-F	22.14	1.242	84.52	23.24
Target-R	22.24	1.251	85.38	23.75

Figure S28. *J-V* curves and photovoltaic parameters of 1.68 eV PSCs with the architecture FTO/Me-4PACz:MeO-2PACz=2:1/$Cs_{0.05}MA_{0.15}FA_{0.8}Pb(I_{0.75}Br_{0.25})_3$/$EDAI_2$/$C_{60}$/BCP/Cu.

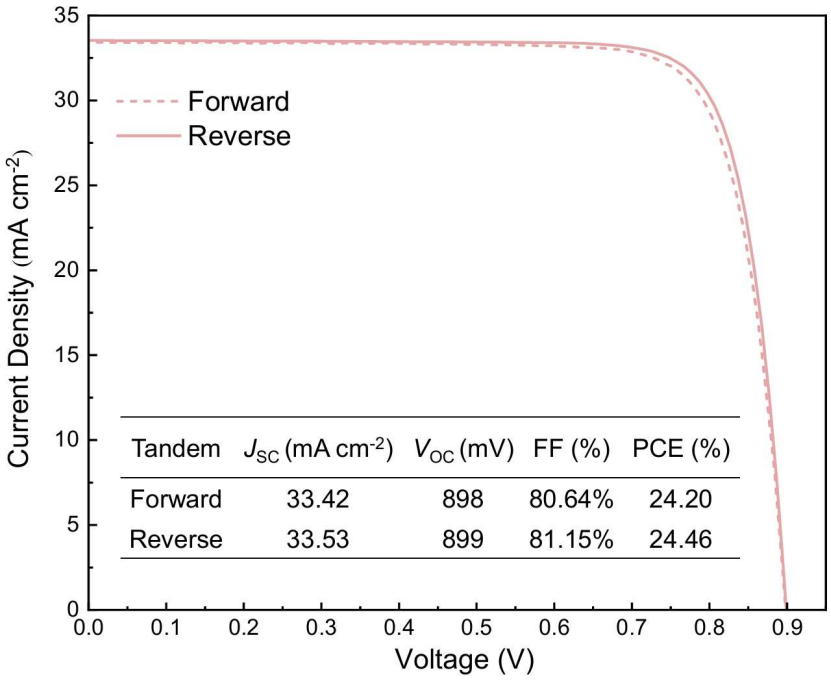

Tandem	J_{SC} (mA cm^{-2})	V_{OC} (mV)	FF (%)	PCE (%)
Forward	33.42	898	80.64%	24.20
Reverse	33.53	899	81.15%	24.46

Figure S29. *J-V* curves and photovoltaic parameters of the 1.25 eV NBG device with the architecture FTO/PEDOT: PSS/$Rb_{0.04}Cs_{0.2}FA_{0.76}Pb_{0.5}Sn_{0.5}I_3$/$EDAI_2$/$C_{60}$/BCP/Cu.

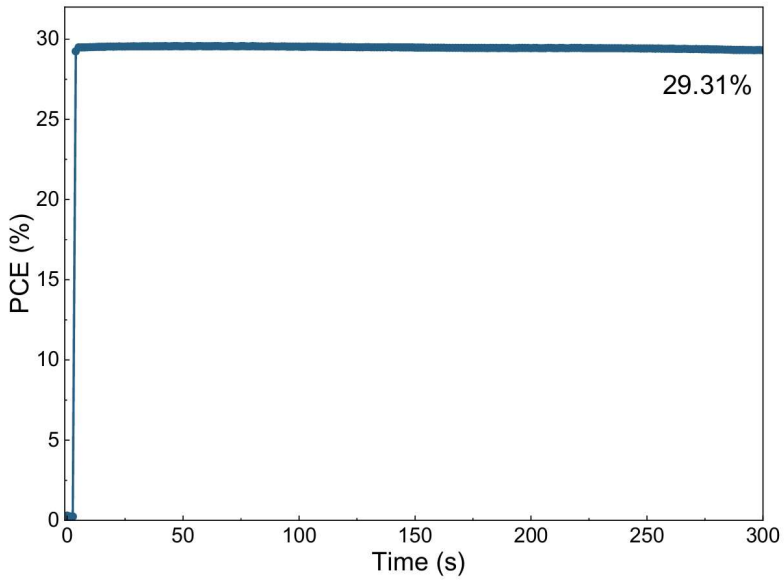

Figure S30. Steady-state power output of the tandem cell during 300 s operation.

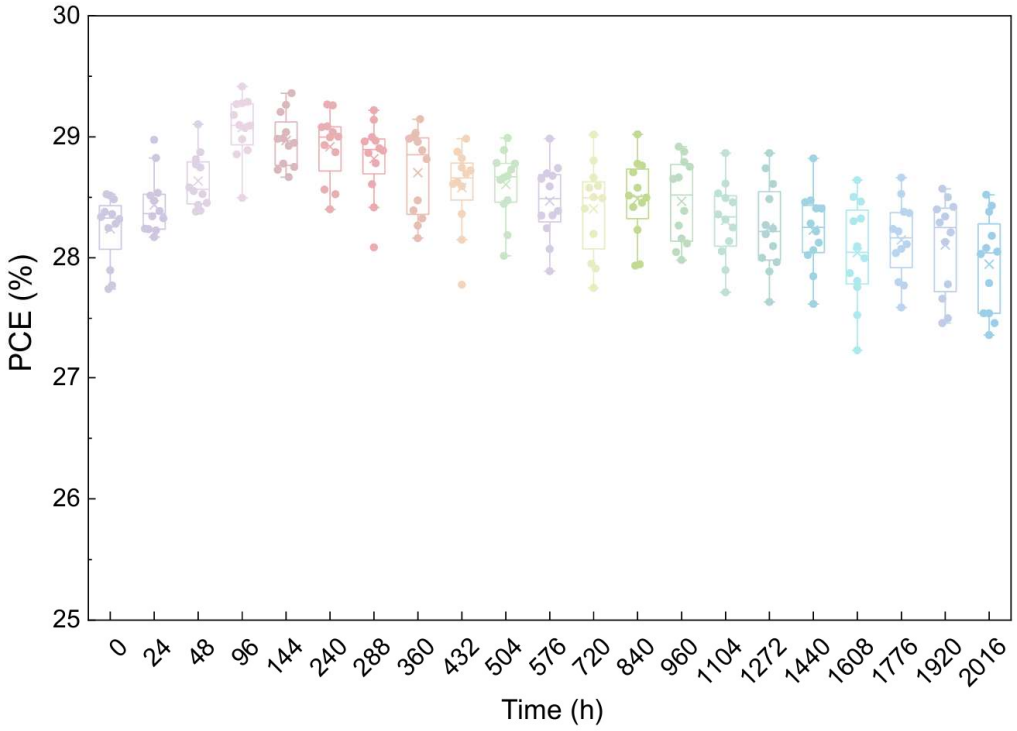

Figure S31. The shelf stability of 12 unencapsulated tandem cells during 2016 hours storage (dark; N_2). Center line, median; cross mark, mean; box range, 25/75 percentiles; whiskers, the outermost outliers within 1.5 × interquartile range. The mean PCEs at 96 h and 2016 h are 29.07% and 27.95%, respectively.

Table S1. Fitting results for the time-resolved PL decay curves. Formula of the double-exponential decay function is $y = A_1*\exp(-x/\tau_1) + A_2*\exp(-x/\tau_2) + y_0$.

Sample	A_1	τ_1 (ns)	A_2	τ_2 (ns)
Control	0.71	128	0.16	576
Target	0.76	228	0.14	750

Table S2. Overlap integrals between the molecular orbitals and perovskite VBM orbital.

Molecular orbital (ψ_m)	Overlap integral $\int \psi_m^* \psi_{VBM} dV$
Me-4PACz HOMO	0.00038
Me-4PACz HOMO-1	0.00040
Me-4PACz/FPT HOMO	0.00112
Me-4PACz/FPT HOMO-1	0.00608

Table S3. Fitting results for the transient absorption decay curves. Formula of the double-exponential decay function is $y = A_1*\exp(-x/\tau_1) + A_2*\exp(-x/\tau_2) + y_0$.

Sample	A_1	τ_1 (ps)	A_2	τ_2 (ps)
Control	0.32	395	0.45	2903
Target	0.33	171	0.48	2690

Table S4. Average photovoltaic parameters with standard deviations of the single-junction PSCs with different FPT consentrations, measured in reverse scan.

Device	J_{SC} (mA cm^{-2})	V_{OC} (mV)	FF (%)	PCE (%)
Control	17.89±0.20	1279±8.84	79.54±1.98	18.20±0.53
0.25 mg/mL	18.18±0.10	1301±7.95	82.90±1.06	19.61±0.37
0.5 mg/mL	18.23±0.19	1305±11.25	84.57±0.77	20.12±0.32
1 mg/mL	18.07±0.13	1301±11.08	82.68±1.01	19.44±0.37

Table S5. Ceritified photovoltaic performance in reverse scan of state-of-the-art WBG PSCs (1.75-1.80 eV).

Year	**Composition**	**E_g (eV)**	**PCE (%)**	**Ref**
2023	$Cs_{0.2}FA_{0.8}Pb(I_{0.65}Br_{0.35})_3$	1.75	18.81	[12]
2024	$Cs_{0.2}FA_{0.8}Pb(I_{0.6}Br_{0.4})_3$	1.77	19.31	[13]
2024	$Cs_{0.2}FA_{0.8}Pb(I_{0.6}Br_{0.4})_3$	1.77	18.88	[14]
2024	$Cs_{0.15}MA_{0.05}FA_{0.8}Pb(I_{0.7}Br_{0.3})_3$	1.75	20.70	[15]
2025	$Cs_{0.2}FA_{0.8}Pb(I_{0.6}Br_{0.4})_3$	1.77	19.72	[16]
2025	$Cs_{0.2}FA_{0.8}Pb(I_{0.6}Br_{0.4})_3$	1.77	19.72	[17]
2025	$Cs_{0.2}FA_{0.8}Pb(I_{0.6}Br_{0.4})_3$	1.77	17.17	[18]
2025	$Cs_{0.2}FA_{0.8}Pb(I_{0.6}Br_{0.4})_3$	1.77	20.21	[19]
2025	$Cs_{0.15}DMA_{0.07}FA_{0.78}Pb(I_{0.7}Br_{0.3})_3$	1.76	21.18	[20]
This work	$Cs_{0.2}FA_{0.8}Pb(I_{0.63}Br_{0.37})_3$	1.76	20.35	

Table S6. Average photovoltaic parameters with standard deviations of the all-perovskite tandem solar cells, measured in reverse scan.

Device	J_{SC} (mA cm^{-2})	V_{OC} (mV)	FF (%)	PCE (%)
Control	15.93±0.18	2068±15.86	82.09±0.97	27.04±0.40
Target	16.24±0.22	2109±16.63	83.48±1.08	28.60±0.52

Reference

1. F. Neese, F. Wennmohs, U. Becker and C. Riplinger, *J. Chem. Phys.*, 2020, **152**, 224108.
2. Y. Zhao and D. G. Truhlar, *Theoretical Chemistry Accounts*, 2008, **120**, 215-241.
3. F. Weigend and R. Ahlrichs, *Physical Chemistry Chemical Physics*, 2005, **7**, 3297.
4. F. Weigend, *Physical Chemistry Chemical Physics*, 2006, **8**, 1057.
5. S. Grimme, J. Antony, S. Ehrlich and H. Krieg, *The Journal of Chemical Physics*, 2010, **132**, 154104.
6. J. PERDEW and Y. WANG, *PHYSICAL REVIEW B*, 1992, **45**, 13244-13249.
7. A. D. Becke, *J. Chem. Phys.*, 1993, **98**, 5648-5652.
8. T. D. Kühne, M. Iannuzzi, M. Del Ben, V. V. Rybkin, P. Seewald, F. Stein, T. Laino, R. Z. Khaliullin, O. Schütt, F. Schiffmann, D. Golze, J. Wilhelm, S. Chulkov, M. H. Bani-Hashemian, V. Weber, U. Borštnik, M. Taillefumier, A. S. Jakobovits, A. Lazzaro, H. Pabst, T. Müller, R. Schade, M. Guidon, S. Andermatt, N. Holmberg, G. K. Schenter, A. Hehn, A. Bussy, F. Belleflamme, G. Tabacchi, A. Glöß, M. Lass, I. Bethune, C. J. Mundy, C. Plessl, M. Watkins, J. VandeVondele, M. Krack and J. Hutter, *The Journal of Chemical Physics*, 2020, **152**, 194103.
9. J. P. Perdew, K. Burke and M. Ernzerhof, *Phys. Rev. Lett. (USA)*, 1996, **77**, 3865-3868.
10. T. Lu and F. Chen, *Journal of Computational Chemistry*, 2012, **33**, 580-592.
11. W. Humphrey, A. Dalke and K. Schulten, *J. Mol. Graph.*, 1996, **14**, 33-38.
12. S. Li, Z. Zheng, J. Ju, S. Cheng, F. Chen, Z. Xue, L. Ma and Z. Wang, *Adv. Mater.*, 2024, **36**.
13. X. Jiang, Q. Zhou, Y. Lu, H. Liang, W. Li, Q. Wei, M. Pan, X. Wen, X. Wang, W. Zhou, D. Yu, H. Wang, N. Yin, H. Chen, H. Li, T. Pan, M. Ma, G. Liu, W. Zhou, Z. Su, Q. Chen, F. Fan, F. Zheng, X. Gao, Q. Ji and Z. Ning, *National Science Review*, 2024, **11**.
14. Z. Yi, W. Wang, R. He, J. Zhu, W. Jiao, Y. Luo, Y. Xu, Y. Wang, Z. Zeng, K. Wei, J. Zhang, S.-W. Tsang, C. Chen, W. Tang and D. Zhao, *Energy Environ. Sci.*, 2024, **17**, 202-209.
15. R. Wang, X. Liu, S. Yan, N. Meng, X. Zhao, Y. Chen, H. Li, S. M. H. Qaid, S. Yang, M. Yuan and T. He, *Nature Communications*, 2024, **15**.
16. D. Pu, X. Zhang, H. Fang, W. Shen, G. Chen, W. Chen, P. Jia, G. Li, H. Guan, L. Huang, Y. Zhou, J. Wang, W. Zheng, W. Meng, G. Fang and W. Ke, *Science Advances*, 2025, **11**.
17. S. Fu, S. Zhou, W. Meng, G. Li, K. Dong, D. Pu, J. Zhou, C. Wang, H. Guan, W. Shao, L. Huang, Z. Su, C. Wang, G. Chen, P. Jia, J. Wang, Z. Xu, X. Gao, H. Cong, T. Wang, C. Xiao, G. Fang and W. Ke, *Nature Nanotechnology*, 2025, **20**, 764-771.
18. X. Zheng, S. Yang, J. Zhu, R. Liu, L. Li, M. Zeng, C. Lan, S. Li, J. Li, Y. Shi, C. Chen, R. Guo, Z. Zheng, J. Guo, X. Wu, T. Luan, Z. Wang, D. Zhao, Y. Rong and X. Li, *Energy Environ. Sci.*, 2025, **18**, 2995-3004.
19. C. Shi, J. Wang, X. Lei, Q. Zhou, W. Wang, Z. Yang, S. Liu, J. Zhang, H. Zhu, R. Chen, Y. Pan, Z. Tan, W. Liu, Z. Zhao, Z. Cai, X. Qin, Z. Zhao, J. Li, Z. Liu and W. Chen, *Nature Communications*, 2025, **16**.
20. Y. Li, X. Zhao, N. Meng, S. Dong, S. Yan, M. Yang, C. Sun, Z. Li, S. Yang, M. Yuan and T. He, *Adv. Mater.*, 2025, DOI: 10.1002/adma.202505694.